Dynamics of the depletion zone at a finite-sized imperfect trap in two dimensions: Photobleaching experiments and simulations

Hailin Peng,[1,*] Sung Hyun Park,[1,†] Panos Argyrakis,[2,‡] Haim Taitelbaum,[3,§] and Raoul Kopelman[1,‖]

[1]*Department of Chemistry, University of Michigan, Ann Arbor, Michigan 48109-1055, USA*
[2]*Department of Physics, University of Thessaloniki, 54124 Thessaloniki, Greece*
[3]*Department of Physics, Bar-Ilan University, Ramat-Gan 52900, Israel*

The kinetics of the growth of depletion zones around a static trap in an effective two-dimensional geometry were studied experimentally with photobleaching of fluorescein dye by a focused laser beam. The phototrap served as an imperfect trap with a finite size. The growth of the depletion zone was monitored by the θ distance, defined as the distance from the trap to the point where the concentration of the reactants reaches a given arbitrary fraction θ $(0 < \theta < 1)$ of its initial value, which could be directly measured experimentally. At the asymptotic limit, the results confirm the theoretical nonuniversal $t^{\theta/2}$ scaling behavior for the θ distance. We also find an effect of fast expansion at an early time of the depletion zone inside an imperfect trap. Both the imperfect trapping strength and the finite trap size are found to control the early-time behavior, while the trap shape does not much affect the dynamics of the θ distance. A dimensional crossover was found for a perfect trap with a finite radius, when the θ distance was measured from the trap surface. The actual trapping efficiency was determined for different laser powers of the phototrap. Results are supported by analytical equations, exact enumerations, and Monte Carlo simulations.

PACS number(s): 82.50.−m

I. INTRODUCTION

The trapping reaction in a diffusion-controlled environment has been studied extensively in the past few decades [1–24]. In this reaction, which can be formulated as $A + T \rightarrow T$, a diffusing species A is annihilated upon collision with a trap T with a certain trapping probability. This process corresponds to the original Smoluchowski work on coagulation [25], which became the basis for classical reaction kinetics theory. Despite the simplicity of the process, the trapping reaction has been one of the most puzzling problems of transport in low-dimensional systems, with many open questions still remaining. Many variations are possible in the trapping problem, such as the number of traps, the trap mobility, or the trapping strength. Previous studies on the trapping reaction in low dimensions include a variety of physical, chemical, or biological processes, such as exciton annihilation in crystals embedded in porous membranes and Vycor glass [2] and the catalytic oxidation of glucose by the enzyme glucose oxidase [3]. The scale of trapping reactions in nature ranges from the atomic level, e.g., electron-hole recombination, to the global level, e.g., the atmospheric ozone depletion.

It is well known that the kinetic laws of diffusion-limited reactions in low dimensions are significantly different [1–24,26–32] from conventional rate laws found in many textbooks [33]. Such anomalous kinetics originates from the inefficient diffusive mixing, which generates the self-segregation of reactants in time. In the trapping reaction in low dimensions, the occurrence of *A-T* reactions creates a zone of depletion around the trap, which is another form of self-segregation of reactants. A number of studies [7–13] have been devoted to the problem of the depletion zone in the vicinity of a single trap.

Among many possible quantities to characterize the dynamics of the depletion zone, the θ distance [10] is a quantity readily observed by experiment. The θ distance r_θ is defined as the distance from the trap T to the point where the concentration of the reactants A reaches a given arbitrary fraction θ $(0 < \theta < 1)$ of its initial value. This can be formulated as

$$c(r_\theta, t) = \theta c_0, \qquad (1)$$

where $c(r, t)$ is the concentration of A particles at distance r at time t, starting from an initial concentration c_0 at time $t = 0$.

In one dimension, the θ distance has been shown, by theory [10] and experiment [8], to increase asymptotically as $t^{1/2}$. In three dimensions, the depletion zone stays localized in the asymptotic time limit and hence the θ distance is time independent. The two-dimensional case produces the most intriguing result of nonuniversality for the θ distance, which is theoretically predicted to scale as $t^{\theta/2}$ at the long-time limit, namely, it depends on the seemingly arbitrary choice of θ [10,12].

In this study, we investigate, by experiment and numerical calculations, a simple case of the trapping problem with a single, static trap surrounded by many diffusing particles in an effective two-dimensional (2D) geometry. Our goal is to provide experimental evidence for nonuniversality in 2D at the long-time limit. The experiment uses a laser beam as a

---

*Email address: peng@umich.edu
†Email address: parksh@umich.edu
‡Email address: panos@physics.auth.gr
§Email address: haimt@mail.biu.ac.il
‖Author to whom correspondence should be addressed. Email address: kopelman@umich.edu
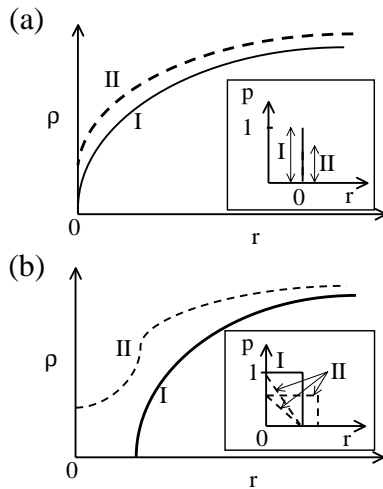
68 061102-1

FIG. 1. Schematic concentration profiles for particles at different types of traps. The profiles of the trapping probability for different traps are shown in the inset. Traps are either a single point, as shown in (a), or nonzero, finite sized, as shown in (b), with the trapping strength either perfect (case I) or imperfect (case II). For a nonzero, finite-sized trap with an imperfect trapping strength [case II in 1(b)], the trap intensity profile can take many different shapes, some of which are shown in the inset.

phototrap, focused onto a sample plane to produce an effective 2D environment. The early-time behavior of the θ distance, which has not been studied previously to our knowledge, is also studied for different trap strengths and trap sizes. Monte Carlo simulations and exact enumerations are performed to support the experimental results. We find that the anomalous early-time behavior exists only for a trap with both an imperfect trap strength and a finite size. An interesting observation of a crossover behavior from 1D to 2D for the θ distance, when measured from the trap surface, is also presented and discussed. Finally, the trapping efficiency κ is determined for different laser powers of the phototrap in the given experiment.

When a finite-sized trap is perfect, the depletion zone is obviously measured from its boundary, as no particles can exist inside. However, when the trap is imperfect, particles can survive within the trap. Then the ''depletion zone'' is actually both inside and outside the imperfect trap perimeter. In this case, measurement of the depletion from the *center* of the trap is a reasonable choice as well.

Figure 1 shows schematic concentration profiles for particles at traps with different size and trapping strength. The insets are the schematics of the corresponding trap intensity profiles. Figure 1(a) represents a point trap with its trapping strength either perfect (case I) or imperfect (case II). Similarly, Fig. 1(b) illustrates a perfect (case I) and an imperfect (case II) trapping strength for a nonzero, finite-sized trap. For a nonzero, finite-sized trap with an imperfect trapping strength [case II in Fig. 1(b)], the trap intensity profile can take many different shapes, a few examples of which are shown in the inset. The perfect trap cases (cases I in Fig. 1) have been well studied so far [7,10,11]. However, studies on the system with an imperfect trap (cases II in Fig. 1) are

limited [9,12], especially for finite trap sizes and in the early-time range inside the finite-sized trap [case II in Fig. 1(b)]. This work focuses on the behavior of the depletion zone at a finite-sized, imperfect trap in 2D as in case II in Fig. 1(b) and its consequences. We find below that the unique shape of the concentration profile profoundly affects the dynamics of the depletion zone at early times.

II. METHODS

A. Experimental setup and procedure

The experiment is the photobleaching of fluorescein dye molecules in a buffer solution using a focused laser beam. The photobleaching occurs inside a small gap between two parallel microscope slides with dimensions $75 \times 25 \times 1$ mm^3. Two optical fibers with a diameter of 150 μm are inserted as spacers between the two parallel microscope slides to produce a small gap with a thickness of 150 μm, which serves as a reaction vessel in this experiment. To minimize the possibility of finite-size effects in the experiment, we positioned the two spacers as far apart from each other as possible between the slides, i.e., 70 mm apart in this case. Fluorescein was chosen for this experiment because the molecule is well known to be easily photobleached by intense excitation light sources.

The aqueous solution of fluorescein was prepared in a phosphate buffer solution at pH 8.5 with a concentration of $7 \times 10^{-5} M$. Spectroscopic grade fluorescein dye was purchased from Aldrich and used without further purification. The phosphate buffer solution was prepared by dissolving monobasic and dibasic potassium phosphate in triply distilled water. The buffer solution was used to increase the solubility of the fluorescein as well as to prevent any potential pH change of the solution during the photobleaching process. The aqueous fluorescein solution was injected into the 150 μm gap between two parallel slides using a glass pipet. After the sample was injected, a sealant (Krytox, DuPont Co.) was applied to the edges of the slides to prevent evaporation of the sample solution during the data acquisition.

A sketch of the setup is shown in Fig. 2(a). A laser beam (see below), focused into a cylindrical shape to produce an effectively two-dimensional environment with a circular trap cross section on the sample plane, is introduced from above the sample chamber to photobleach the dye molecules. The size of the focused laser beam on the sample plane is approximately 60–80 μm in radius. Two different laser powers have been used to check the effect of the trap strength, one at 12 mW from a 488 nm beam out of an air-cooled Ar-ion laser (Ion Laser Technology, model no. 5490 AWC-0), and the other at 130 mW at 430 nm out of a frequency doubler (Spectra-Physics, model no. GWU-23FS) coupled with a femtosecond Ti-sapphire laser (Spectra-Physics, Tsunami, model no. 3941-L1S). Another light source at 480$\pm$5 nm with approximately 1 in. diameter from a mercury lamp (Ushio, model no. USH-102D), illuminating from below, was used to probe the progress of the photobleaching. The power density of the probe beam is less than 0.1% of that of the photobleaching laser beams, so the effect of photobleach-
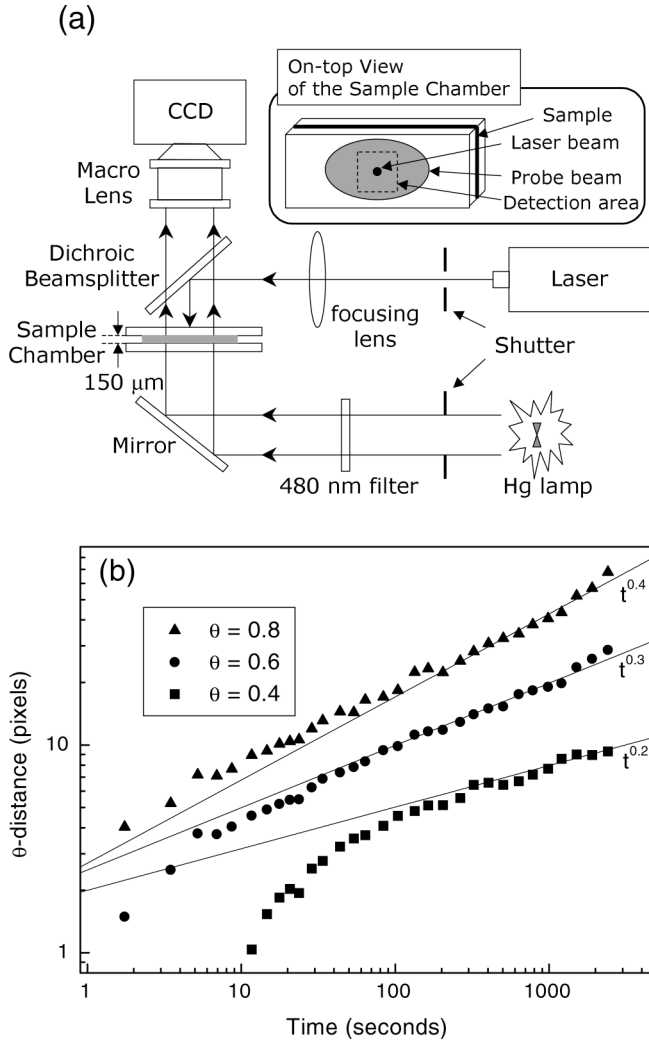
(a)

(b)

FIG. 2. (a) A schematic diagram of the experimental setup. (b) A plot of θ distance vs time from experiment. The θ distance is measured at $\theta = 0.4$, 0.6, and 0.8. Note that the θ distance, growing as $t^{\theta/2}$ asymptotically, shows a nonuniversal behavior. Also note that, for $\theta = 0.4$ and 0.6 at early times, the θ distance near the center of the trap grows at a much faster rate before converging to the asymptotic rate.

ing by the probe beam can be neglected during the typical time scale of the experiment. Two mechanical shutters, installed in front of the light sources, operate out of phase, so that the photobleaching beam and the probe beam are illuminating the sample alternately in time.

The images of fluorescence emission from the sample were collected at different times, using a charge-coupled device (CCD) camera (Spectra Source Instruments, model Teleris 2 12/16) equipped with a macro lens (Nikon, AF Macro 60 mm f2.8, 1:1). The scale of the image is 1×1 cm^2 with a 512×512 pixel resolution. Typical integration time of the CCD is 4 s for each image. The dye molecules become *invisible* to the detector when photobleached, resulting in a drop in the fluorescence intensity.

The progress of the photobleaching was followed for 1 h in a typical experiment. The entire experiment is performed at room temperature. A similar experimental setup has been used recently to study the trapping reaction in one dimension [8].

B. Monte Carlo simulations

The simulation calculations are performed using well-known numerical techniques for random walks and for trapping on a 2D square lattice with a single trap site positioned in the center. The trapping probability p for this site is a parameter varying from 0 to 1, i.e., $0 < p < 1$. All other sites are equivalent sites, while only the single trap site has the trapping properties. A number of particles are randomly positioned on the lattice, with a given concentration c_0. No more than one particle is allowed to occupy a given site at any moment. No particles are allowed initially to land on the trap site.

The diffusion is modeled by random walks of all particles, which are independent of each other. We use cyclic boundary conditions at the ends of the lattice. If a particle is chosen to move to a site that is already occupied by another particle, then this move is not allowed. If a particle happens to occupy the middle (trap) site during a move, then it is trapped with a probability p. This is done as usual by drawing a random number and comparing this number with p. If the particle is trapped, then it is removed irreversibly from the lattice, and, therefore, the particle concentration on the lattice is reduced. If it is decided that it is not to be trapped, then the particle remains on the trap site and continues to perform its random walk, similarly to all other particles and sites.

The quantity that we monitor is the number of particles at a distance r from the origin (i.e., from the trap site). Since we use a discrete two-dimensional square lattice topology, we used the quantity $|i| + |j|$ as the value of r, for the position at (i,j) on the lattice. For a fixed time step, we count the total number of particles at each distance on the lattice. Then the number of particles is normalized into a concentration to measure the θ distance. The data are the average of 20 000 runs, unless mentioned otherwise.

C. Recursion formula calculation

The following recursion formula is used to numerically calculate the exact particle concentration $c(i,j;t)$ at a lattice position (i,j) at a time step t on a two-dimensional square lattice, where an imperfect trap of radius a with a trapping probability p is located in the middle of the lattice:

$$c(i,j;t) = [c(i-1,j;t-1) + c(i+1,j;t-1) + c(i,j-1;t-1)$$
$$+ c(i,j+1;t-1)]/4, \qquad (2a)$$

with the initial condition of uniform spatial distribution of particles

$$c(i,j;t=0) = c_0, \qquad (2b)$$

and the trapping boundary condition

TABLE I. Recursion relationships of $c(i,j;t)$, a reactant concentration at position (i,j) $(i,j=$ integer) at time t $(=0, 1, 2,...)$, in exact 2D and quasi-2D. We assume the space and time to be discrete, and all the particles are forced to move randomly at each time step. The trap location is at $(0, 0)$ in exact 2D, and $(0, 0, k)$ $(k=$ integer) in quasi-2D. IC denotes initial condition, BC boundary condition; p is the trapping probability. The forms of the BC for imperfect traps reflect the radial symmetry around $(0,0)$.

System	Recursion relation	IC, $c(i,j;0)$	BC, $c(0,0;t)$, $t\neq0$	
Exact 2D	$C(i,j;t)=[c(i-1,j;t-1)+c(i+1,j;t-1)$ $+c(i,j+1;t-1)+c(i,j-1;t-1)]/4$	c_0 (const)	Perfect	0
			Imperfect	$(1-p)[c(1,0;t-1)]$
Quasi-2D	$C(i,j;t)=[c(i-1,j;t-1)$ $+c(i+1,j;t-1)+c(i,j+1;t-1)$ $+c(i,j-1;t-1)]/6+c(i,j;t-1)/3$	c_0 (const)	Perfect	0
			Imperfect	$(1-p)[2c(1,0;t-1)+c(0,0;t-1)]/3$

$$c(i,j;t)=(1-p)[c(i-1,j;t-1)+c(i+1,j;t-1)$$
$$+c(i,j-1;t-1)+c(i,j+1;t-1)]/4$$
$$\text{for } |i|+|j|\leq a, \tag{2c}$$

where i, j are integers, and $t=0,1,2,...$. Equation (2a) implies a forced random walk on a 2D lattice, i.e., the particle concentration at a position (i,j) at time step t solely depends on the concentrations at the four nearest neighbor locations at the previous time step $t-1$, with each nearest neighbor contributing an equal probability of 1/4.

The recursion formula in quasi-2D on a cubic lattice, shown in Table I, can be derived in a similar way. "Quasi-2D" is a 3D infinite cubic lattice on which particles have coordinates (i,j,k), and a trap is located on an axis along the k direction. Due to the symmetry along the k direction, only two indices (i,j) are needed to represent the concentration in quasi-2D. More details on the derivation of the recursion formula are described elsewhere [8,34].

D. Analytical approach

The exact solution for the diffusion equation governing the diffusion of A particles in a two-dimensional region bounded internally by the trapping circle $r=a$ is given by [12,34]

$$c(r,t)=-\frac{2\kappa c_0}{\pi}\int_0^\infty e^{-Dtu^2}\frac{J_0(ru)[uY(au)+\kappa Y_0(au)]-Y_0(ru)[uJ_1(au)+\kappa J_0(au)]}{[uY_1(au)+\kappa Y_0(au)]^2+[uJ_1(au)+\kappa J_0(au)]^2}u^{-1}du, \tag{3}$$

where $J_o(z)$, $J_1(z)$, $Y_0(z)$, and $Y_1(z)$ are Bessel functions, c_0 is the bulk concentration, D is the diffusion coefficient, a is the radius of the trap, and κ is a parameter representing the strength of the trap, ranging from 0 for to a total reflection (i.e., no trapping) to ∞ for a total absorption (i.e., perfect trapping).

The approximate analytical expressions for the concentration profile at the short- and long-time limits have been derived [12] from Eq. (3), from which one can obtain the θ distance. For the perfect trap, with radius a, it has been shown [12] that, in the short-time limit,

$$c(r,t)\approx c_0\left[1-\left(\frac{r}{a}\right)^{1/2}\text{erfc}\left(\frac{r-a}{\sqrt{4Dt}}\right)+\cdots\right], \tag{4a}$$

and in the long-time limit,

$$c(r,t)\approx 2c_0\ln\left(\frac{r}{a}\right)\left[\frac{1}{\ln(4T)-2\gamma}-\frac{\gamma}{[\ln(4T)-2\gamma]^2}+\cdots\right], \tag{4b}$$

where $T\equiv Dt/a^2$ is the dimensionless time parameter, and $\gamma=0.57722...$ is Euler's constant. We calculated the concentration profiles numerically from Eqs. (4a) and (4b), for an arbitrary diffusion constant $D=1$ and a trap radius $a=1$, and then measured the θ distance from the profiles. This approach, with time and space being continuous, allows one to investigate the behavior of the θ distance at an extremely short time when the depletion zone is located in the vicinity of the trap boundary.

III. RESULTS AND DISCUSSION

A. Nonuniversal asymptotic behavior

A series of typical fluorescence images from the photobleaching experiments are presented elsewhere [13]. The growth of the depletion zone is detected by the decrease in the fluorescence intensity around the trap in time. After background subtraction and division by the initial fluorescence intensity, the fluorescence intensity along a single arbitrary pixel line through the trap center is converted into the spatial profile of the fraction of reactant molecules remaining at each time. These are presented in [13]. The θ distance was measured directly from such a spatial density profile at each time.
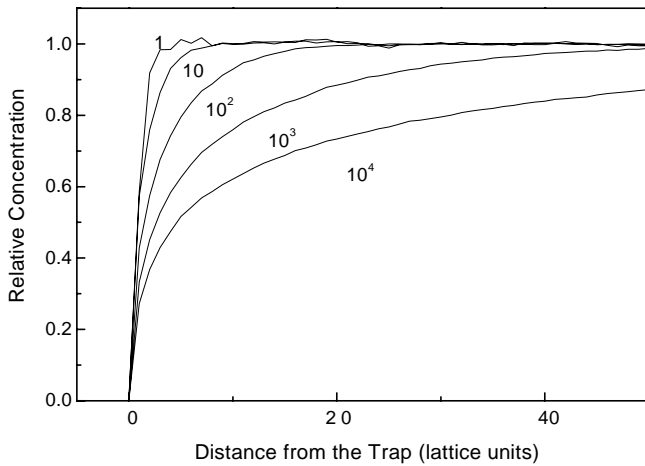
FIG. 3. Spatial profiles of the fraction of initial particle concentrations at select time steps $t = 1$, 10, 10^2, 10^3, and 10^4 for a perfect point trap in exact 2D, obtained from a Monte Carlo simulation. The trap is a single point located at the center of a 201×201 square lattice, and the initial concentration of particles is 0.25. Cyclic boundary conditions are used and the data are the average of 20,000 runs. The initial ($t = 0$) concentration is normalized to unity.

Figure 2(b) shows the θ distance vs time on a logarithmic scale, measured at $\theta = 0.4$, 0.6, and 0.8, from the experimental data. The solid lines in the plot represent the theoretical asymptotic slopes of the θ distance for a perfect trap in 2D, i.e., the slopes of $\theta/2$. The experimental data fit very well with the theoretical slopes in the long-time limit. All the data seem to reach the asymptotic limit after ~ 300 s under the present experimental conditions. This result confirms that the θ distances at different θ values develop with different time scaling in 2D geometry [10,11].

The nonuniversal scaling of the θ distance in 2D trapping implies a slower widening of the depletion zone for smaller θ values, resulting in a curved shape of the density fraction profile, which is getting very narrow at lower fractions, around the trap, as shown in Fig. 3. This is very different from the case of 1D trapping, where the shape of the fraction profile is much broader and nearly straight near the trap [8], since the depletion zone grows at a uniform rate of $t^{1/2}$ for all θ values in 1D. In other words, the depletion zone opens up faster in 1D than in 2D for the trapping process, and the difference is more pronounced near the trap at a lower density fraction at a given time, where the diffusing particles in 2D are not depleted as fast as in 1D.

We note that there is a finite amount of dye molecules inside the trap at all times in our experiment, because the phototrap with a finite laser power cannot bleach all the dye molecules instantly. This implies that the phototrap in our experiment is a finite-sized imperfect trap, which allows the dye molecules to escape at a certain, finite probability. The excellent match of the experimental data with the theory in the long-time range in Fig. 2(b) suggests that in the asymptotic limit the theory for the system with a perfect trap is also valid for the one with a finite-sized, imperfect trap. This is also borne out by simulations below.
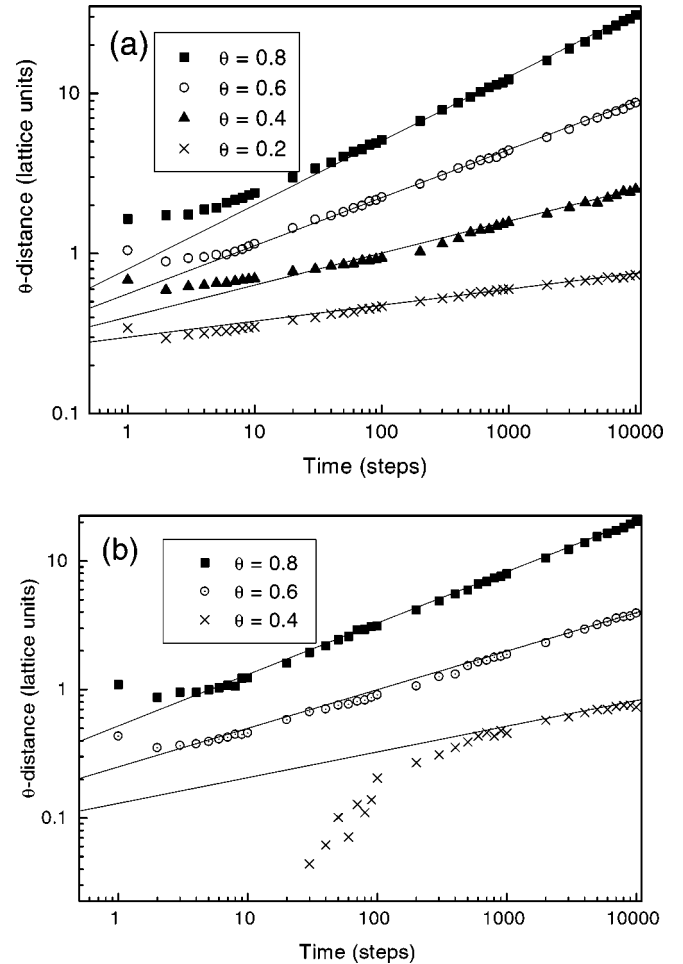

FIG. 4. Plots of θ distance vs time from Monte Carlo simulations, (a) for a perfect point trap in exact 2D, at $\theta = 0.2$, 0.4, 0.6, and 0.8, obtained from the profiles in Fig. 3, and (b) for an imperfect point trap with a trapping probability $p = 0.5$, in exact 2D, at $\theta = 0.4$, 0.6, and 0.8. Solid lines represent the theoretical, nonuniversal slope of $\theta/2$ at the asymptotic limit. Both results show excellent agreement with the theoretical values at long times. Note that the high-slope, early-time behavior near the trap center for lower θ's, which was observed from experiment, is reproduced for $\theta = 0.4$ in the case of the imperfect point trap only, while the early-time deviation is completely missing in the perfect point trap case. The initial ($t = 0$) concentration is normalized to unity.

B. Anomalous early-time behavior

Figure 2(b) also shows that, for short times near the trap origin, the θ distance grows faster than the asymptotic rate for smaller θ values (i.e., at $\theta = 0.4$ and 0.6). It also seems that there is no well-defined time scaling for this behavior. To our knowledge, such a fast-growing, early-time behavior has not been predicted or reported previously. Noting that the experimental phototrap has properties different from the theoretical perfect point trap model, such as the imperfect trap strength, finite trap size, and nonuniform trap strength inside the trap, we conjecture that the apparently anomalous early-time behavior from our experiment comes from the imperfect nature of the phototrap. We investigate this behavior systematically by using a set of numerical simulations with various techniques, as follows.
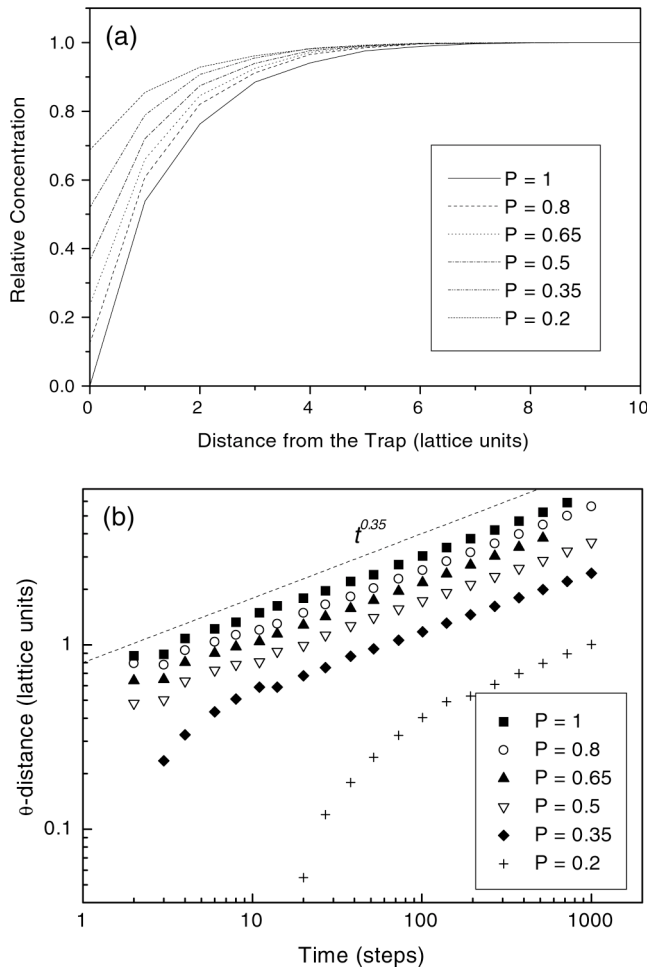
FIG. 6. A plot of θ distance vs time, for different trap sizes, at a fixed θ value of 0.4, from recursion formula calculations. Solid line represents the upper limit radius of each trap. A trap with radius a is located on a 2D square lattice. The trapping probability is uniform at $p=0.5$ inside the trap, for all trap sizes. Trap size of $a=1$ represents a point trap. Note that the high-slope, early-time behavior appears only inside the trap for all trap sizes.

for the case of the imperfect point trap from the Monte Carlo simulations, in which the only apparent difference is the non-zero, finite reactant concentration at the origin at all times.

We measured the θ-distance at $\theta=0.2$, 0.4, 0.6, and 0.8 from the profiles in Fig. 3 (and many more profiles at other time steps not shown), which are represented as symbols in Fig. 4(a). The solid lines are the theoretical slopes of $\theta/2$ at the asymptotic limit. Figure 4(b) is a similar plot for an imperfect point trap with a trapping probability 0.5 at the trap and zero elsewhere. Both cases, regardless of the difference in trap strength, match the theoretical asymptotic scaling very well in the long-time limit, which is consistent with the experimental result in Fig. 2(b). Furthermore, Fig. 4 shows directly that the fast-growing, early-time behavior is reproduced only for the imperfect point trap. For the perfect point trap in Fig. 4(a), the θ distance remains almost constant at the first few time steps, then grows faster gradually, until the asymptotic growth rate is reached. In this case, the early-time slope is always smaller than the asymptotic one, and there is no region where the depletion zone grows at a faster rate than the asymptotic one. On the other hand, for the imperfect point trap in Fig. 4(b), the θ distance grows at a much higher rate than the asymptotic one, for $\theta=0.4$ at early times, and then gradually slows down to the asymptotic rate in the long time range. Such a fast, early-time behavior does not exist for the higher θ values in Fig. 4(b), which also matches with the experimental observation in Fig. 2(b). This result suggests that the trap strength as well as the θ value is an important factor in the early-time growth of the depletion zone.

To study the effect of trap strength on the growth of the depletion zone more systematically, we performed numerical calculations for various trap strengths, using the recursion formula in Table I. Figure 5(a) shows the concentration profiles for different trapping probabilities, at a fixed time step $t=20$, for a system where a trap is located at a single lattice

FIG. 5. (a) Spatial concentration profiles at a fixed time step $t=20$, for different trapping probabilities, from recursion formula calculations, for a point trap in exact 2D. A point trap with a corresponding trapping probability is located at the center of a 2D square lattice. The horizontal axis represents the distance from the trap center. As the trapping probability increases, the particle concentration becomes lower at and near the trap, leading to the broader depletion zone at a given time. The initial ($t=0$) concentration is normalized to unity. (b) A plot of θ distance vs time, for different trapping probabilities, at a fixed θ value of 0.7, measured from the concentration profiles in (a). The dashed line represents the theoretical asymptotic slope 0.35. Note that the high-slope, early-time behavior appears more clearly as the trapping probability becomes smaller.

1. Effect of trap strength

Figure 3 shows the normalized concentration profiles as a function of the distance from the trap at the origin, obtained from a Monte Carlo simulation. A trap, with a trapping probability 1, is located at a single lattice site on a 201×201 square lattice, while everywhere else on the lattice there is zero trapping probability. The initial concentration of the particles is 0.25. The data in the plot represent the results at time steps $t=1$, 10, 10^2, 10^3, and 10^4. The particle concentration is zero at the origin at all times, reflecting the perfect trapping. We call this trap a *point* trap, because it occupies only one lattice site. We obtained similar concentration profiles
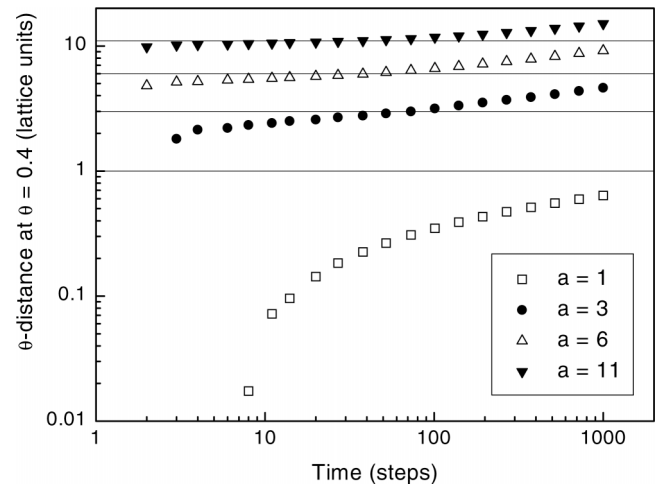
site on a 2D square lattice. As expected, the particle concentration becomes lower in the vicinity of the trap, as the trapping strength increases, at a given time. Figure 5(b) shows the θ distance measured at $\theta = 0.7$ from these concentration profiles. All θ distances from different trap strengths reach the asymptotic scaling of $t^{0.35}$, confirming our earlier conclusion that the asymptotic behavior does not depend on the trap strength. However, we note that the fast-growing, early-time behavior appears only at the lower trapping probabilities, i.e., for trapping probabilities below 0.5 in Fig. 5(b). Traps with higher probabilities do not show such a fast-growing, early-time behavior, even though their trapping probability is less than 1. This result suggests that the trap strength cannot completely explain the existence of the fast, early-time behavior. We find, below, that the trap size is another factor, which affects the early-time dynamics of the depletion zone. The difference for $\theta = 0.6$ in the early-time range between Figs. 2(b) and 4(b) can be understood in terms of such an effect.

2. Effect of trap size

With a closer look at the values of the θ distance in Fig. 2(b), one realizes that the fast-growing, early-time behavior occurs roughly at a θ distance below 3–4 pixels. Noting that the radius of the phototraps in our experiments is approximately 60–80 μm, which corresponds to 3–4 CCD pixels, one finds that such an anomalous early-time behavior occurs only *inside* the trap. A similar trend is found in the numerical results in Figs. 4(b) and 5(b), where only those θ distances smaller than one lattice constant show the fast-growing, early-time behavior. This observation suggests that the trap size, too, should play an important role in the anomalous, early-time behavior. Although the traps in Figs. 4(b) and 5(b) occupy only a single lattice point, and are thus called *point* traps, it is important to realize that the size of such a point trap is not necessarily zero, because the space is discrete in the lattice model. In fact, it is reasonable to assume that the effective radius of a point trap is about half a lattice distance in a discrete lattice space. Furthermore, the effective radius of a point trap in lattice space may also depend on the trap strength. Hence, some of the θ distances smaller than 1 in Figs. 4(b) and 5(b) can be regarded as a measure of the depletion zone *inside* the trap.

To support the above argument, we carried out numerical calculations using the recursion formula, extending the trap size. The systems examined are traps with various radii, with a uniform trapping probability of $p = 0.5$ inside the trap, located on a 2D square lattice. Figure 6 summarizes the results. The figure presents the time evolution of the θ distance for different trap sizes, measured at a fixed θ value of 0.4, from the recursion formula calculations. Solid lines represent the upper limit of the radius of each trap studied. The upper limit radius of 1 represents a point trap, for which the trap radius lies between 0 and 1, as explained in the previous paragraph. It clearly shows that the fast, early-time behavior appears only below the upper limit of the trap radius. It confirms that the high-slope, early-time growth of the depletion zone occurs only inside the trap.

The results so far suggest that the fast, early-time growth of the depletion zone occurs in systems with an imperfect, finite-sized trap, inside which a certain fraction of particles can exist. As the depletion zone at a certain fraction opens up to the "outside" of the trap, the θ distance at that specific fraction becomes bigger than the trap radius, and its growth slows down to converge to the asymptotic rate. Conversely, one can determine the effective size of the trap by measuring that θ distance where the transition occurs from the early-time regime of fast expansion of the depletion zone to the asymptotic regime. In Fig. 4(b), for example, the transition from the higher slope to the asymptotic slope occurs at a θ distance around 0.3, suggesting the "effective" trap size of the point trap in this case to be approximately 0.3.

3. Effect of trap shape

The phototrap in our experiments, created by focusing the laser beam, has a nonuniform intensity distribution across the trap area, most likely with a Gaussian profile. As a final check on the imperfect nature of the phototrap, we examined the effect of the trap shape, i.e., the distribution of the trapping probability across the trap area, on the dynamics of the θ distance, using the calculations via recursion formula. Figures 7(a)–7(d) show the concentration profiles obtained from the exact enumerations for different trap shapes. The inset shows the trap shape. Figure 7(a) is the simplest "point" trap, with p, the trapping probability, being 0.5 at the trap and 0 elsewhere. Figures 7(b)–7(d) represent a "Lorentzian" trap, a "Gaussian" trap, and a "rectangular" trap, respectively. Details of the distribution of the trapping probability for each trap are described in the figure caption. By comparing the concentration profiles from different trap shapes, one can notice a common trend: the concentration profiles inside the trap resemble the shape of the trap at early times. Then, as the concentration inside the trap decreases in time, all profiles become convex [see Fig. 7(c) for the definition of the curvature], which is obviously the result of the diffusion of the particles from the outside into the trap. In this sense we may call the early-time range trapping dominant, and the long-time range diffusion dominant. This is a special case of reaction- vs diffusion-limited chemical kinetics [14,15].

When the trap shape is concave, e.g., the Lorentzian trap in Fig. 7(b), the curvature of the concentration profile inside the trap changes from concave to convex in time. We find that such a curvature change in concentration profile does not affect the dynamics of the θ distance. In fact, we find that the dynamics of the θ distance is not affected by the details in the shape of the trap at all. The θ distance measured from Fig. 7(d) is shown in Fig. 8, where the fast-growing, early-time regime appears inside the trap, just like the results in Figs. 2(b), 4(b), and 5(b). Similar results were obtained from the other trap shapes in Fig. 7.

4. Crossover from 1D to 2D

Figure 9(a) presents the θ distance for a perfect trap with a radius 1, in a continuous 2D space, obtained from the numerical calculations using Eqs. (4a) and (4b). Solid lines
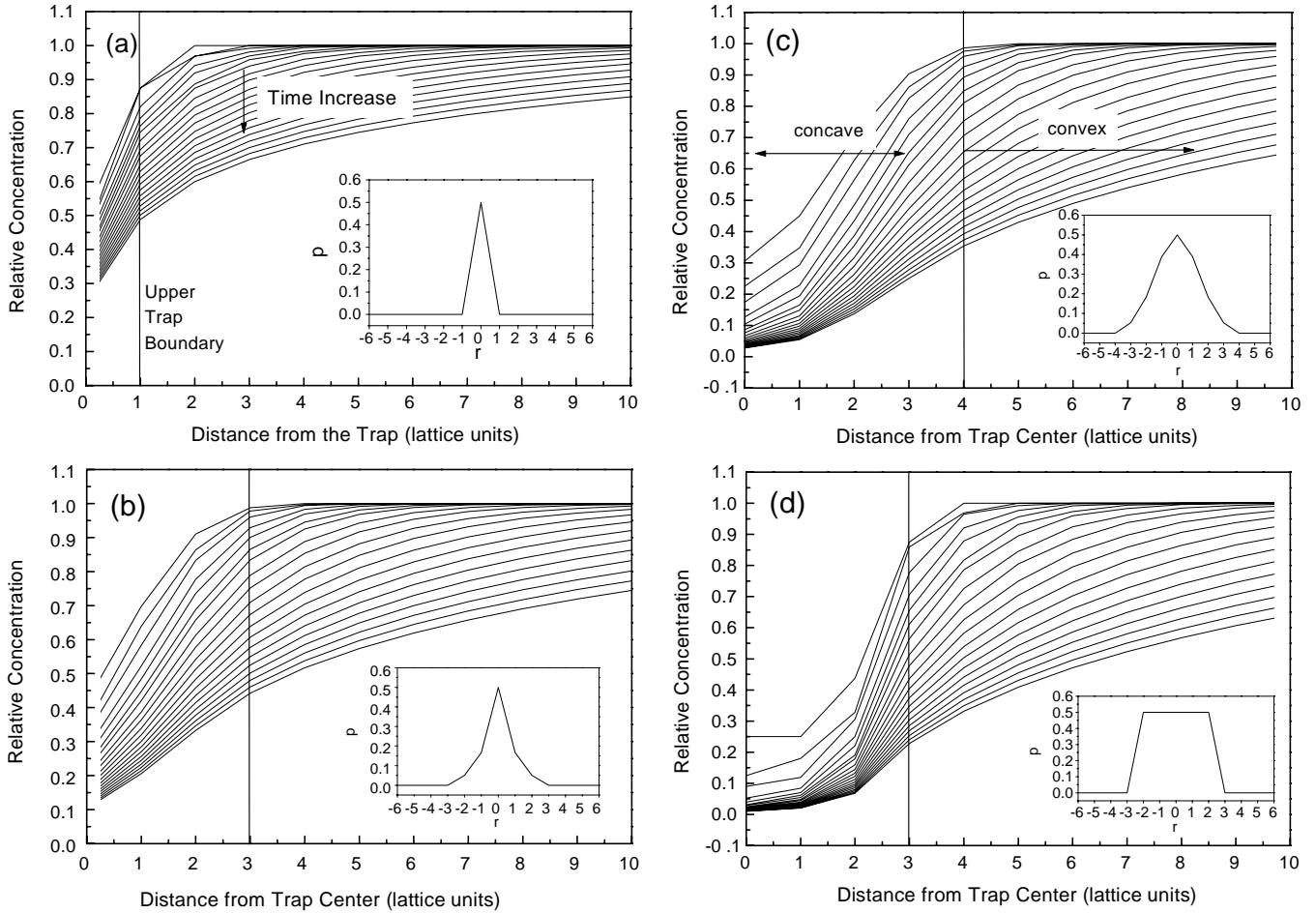
FIG. 7. Concentration profiles for different trap shapes. The trap shape is shown as an inset for each profile. (a) A point trap, with a trapping probability $p = 0.5$ at a single lattice site; (b) a Lorentzian trap, where $p = 0.5$ at the peak position, 0.17 at the nearest neighbor, and 0.050 at the second nearest neighbor; (c) a Gaussian trap, where $p = 0.5$ at the peak position, 0.39 at the nearest neighbor, 0.184 at the second nearest neighbor, and 0.053 at the third nearest neighbor, and (d) a rectangular trap, where $p = 0.5$ at all positions inside the trap. The trapping probability is zero elsewhere. The initial ($t = 0$) concentration is normalized to unity.
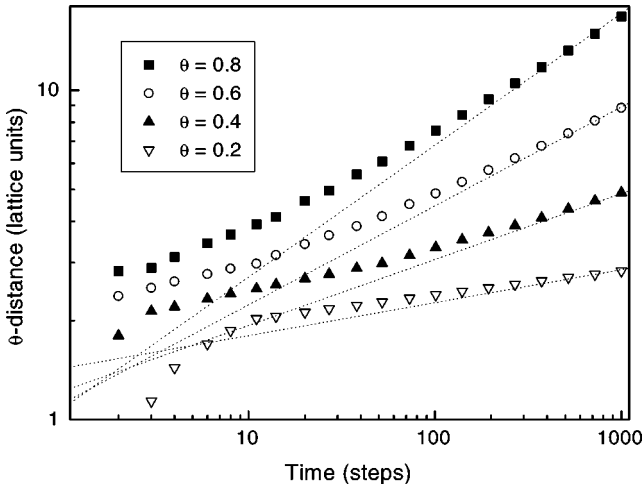

FIG. 8. A plot of θ distance vs time for the rectangular trap, measured from the concentration profiles in Fig. 7(d). Dashed lines represent the theoretical slopes at the asymptotic time limit in 2D.

represent the theoretical asymptotic time scaling in 2D. As expected, the θ distance, which is always bigger than the trap radius in this case, increases slowly in time, until it reaches the asymptotic slope of $\theta/2$. There is no fast-growing, early-time behavior in this case, because the trap is perfect and no particle can survive inside the trap. However, when the θ distance is measured from the trap surface, instead of the center of the trap, we obtain an interesting result, as shown in Fig. 9(b). In this case, the θ distance starts with a universal 1D scaling of $t^{1/2}$ for all θ's at early times, before it crosses over to a nonuniversal 2D scaling of $t^{\theta/2}$. This result can be interpreted as follows. At early times, when the particles are in the vicinity of a trap, they are affected by only a small part of the 2D trap surface, as if it was a 1D trap. In other words, the particles, located at a much closer distance than the size of the trap (i.e., the distance from the particles to the trap surface is much less than the trap size), are not affected by the entire shape of the trap. At later times, when the particles are far enough from the trap (i.e., the distance from the particles to the trap surface is much greater than the trap size), the 2D nature of the trap finally affects then, thus changing
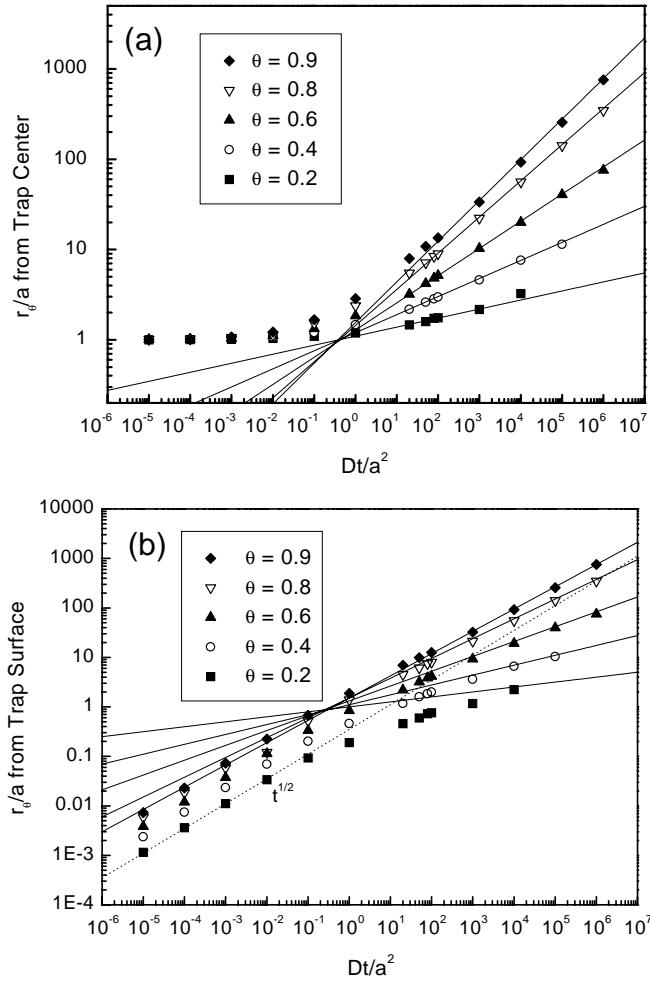
FIG. 9. A plot of the θ distance in the unit of the trap radius a vs dimensionless time Dt/a^2 for the perfect trap with radius $a=1$, in spatially and temporally continuous 2D, obtained from Eqs. (4a) and (4b). The θ distances are measured from (a) the center of the trap, which reproduces the results from Monte Carlo simulations and recursion formula calculations, or (b) the surface of the trap, which shows a dimensional crossover from 1D to 2D. The theoretical asymptotic slopes for 2D are shown as solid lines, and for 1D as a dashed line.

the dynamics accordingly. This argument can be extended to the case of a spherical trap in 3D as well: the depletion zone will develop as for the 1D case, in the beginning near the trap surface, before it is eventually affected by the entire sphere and stops growing (3D). This is a useful idea to explain the early-time growth of the depletion zone outside the trap. We note that moving the origin of the coordinate system to the edge of the perfect trap system shows the crossover in a more transparent way. Obviously, for a perfect trap it is the edge that controls the trapping, with the center not playing any role.

According to the above argument, we can also predict the following: in a given trapping system, the crossover from 1D to 2D (or 3D) occurs faster for larger θ, because the larger θ distance (corresponding to the larger θ at a given time), is affected by the entire trap faster than is the smaller θ dis-
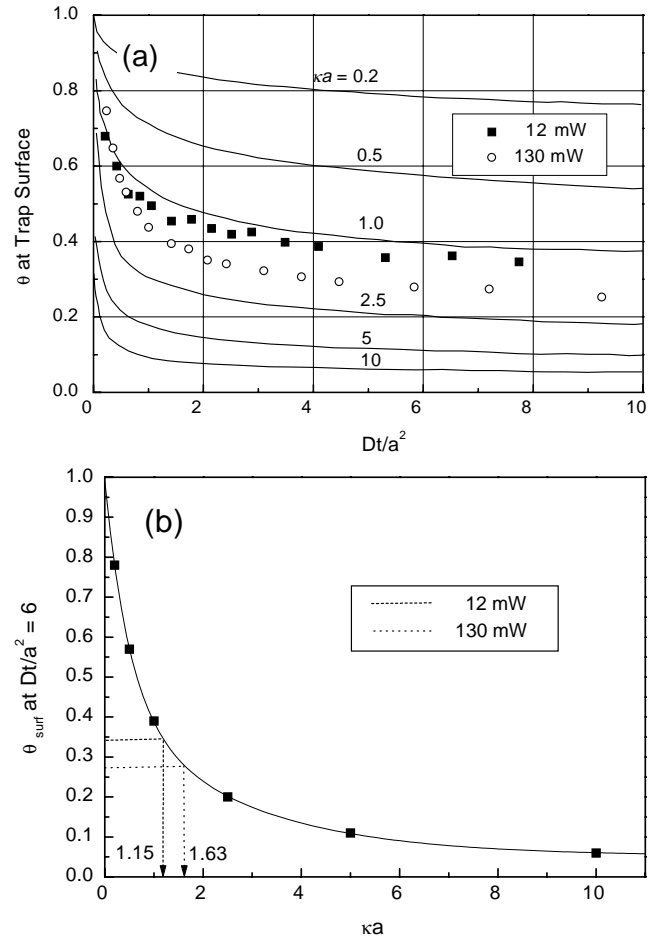

FIG. 10. (a) A plot of the fraction θ of the reactants at the trap surface (θ_s) vs Dt/a^2, for various values of κa in 2D. Solid lines represent the theoretical values from Eq. (3). The experimental data with different laser powers are shown as solid squares (12 mW) and open circles (130 mW). (b) A plot of θ_s vs κa at $Dt/a^2=6$, from (a). The value of κa for each trapping laser power from experiments is determined, as shown by the arrows.

tance. This prediction can be readily verified from Fig. 9(b), i.e., the dimensionless crossover time Dt_c/a^2 is $\sim 10^{-3}$ for $\theta=0.8$, while it is ~ 10 for $\theta=0.2$.

IV. EXPERIMENTAL DETERMINATION OF TRAPPING STRENGTH

As a practical application of this study, one can extract the value of the theoretical trapping efficiency κ [12] for the laser phototrap used in the experiments. Trapping efficiency is a measure of the trap strength, ranging from zero for no trapping to infinity for a perfect trapping. Note that the trapping efficiency κ, with a dimension of $(length)^{-1}$, is the continuous analog of the trapping probability p, which varies between 0 (no trapping) and 1 (perfect trapping). The reactant concentration at the trap surface depends only on the trapping efficiency κ [34]. Using the diffusion constant of the reactant (in this case, $D=4.37\times10^{-6}\ cm^2\,s^{-1}$ for

fluorescein [35]), the trap radius a (60–80 μm), and the concentrations measured experimentally at the trap surface, one can calculate the trapping efficiency κ for a given laser power by comparing with the theoretical values of the reactant concentrations at the trap surface, which can be obtained from Eq. (3). Figure 10(a) is a plot of the concentration fraction at the trap surface (θ_s) vs Dt/a^2, for various theoretical κa values and the experiments with fluorescein using different laser powers. Solid lines represent the theoretical values calculated from Eq. (3), and the experimental data with different laser powers for the phototrap are shown as solid squares (12 mW) and open circles (130 mW). The experimental data follow the theoretical trend very well. Figure 10(b) is a plot of θ_s vs κa at $Dt/a^2 = 6$, from Fig. 10(a). The κa value for each laser power is determined to be 1.15 for 12 mW and 1.63 for 130 mW, respectively. Considering that the power density of the laser beam is calculated as 1.1 W/mm^2 for the 12 mW beam and 6.5 W/mm^2 for the 130 mW beam, at the focus on the sample plane, we note that the theoretical trapping efficiency κ is not linearly proportional to the laser power density.

V. SUMMARY

We present experimental evidence for the theoretically predicted nonuniversality in the growth of the depletion zone at the asymptotic limit in 2D. We find that the trap strength does not affect the asymptotic behavior of the θ distance. A fast, early-time behavior is shown to exist inside a finite-sized trap with an imperfect trapping strength. The trap shape does not seem to change the dynamics of the θ distance. A dimensional crossover was clearly observed when the origin of the θ distance measurement was shifted from the trap center to the trap surface. The theoretical trapping efficiency was determined for different laser powers of the phototrap. The results are consistent with numerical calculations using various techniques.

[1] F. den Hollander and G. H. Weiss, in *Contemporary Problems in Statistical Physics*, edited by G. H. Weiss (SIAM, Philadelphia, 1994).

[2] R. Kopelman, S. Parus, and J. Prasad, Chem. Phys. **128**, 209 (1988).

[3] A. L. Lin, M. S. Feldman, and R. Kopelman, J. Phys. Chem. B **101**, 7881 (1997).

[4] J. K. Anlauf, Phys. Rev. Lett. **52**, 1845 (1984).

[5] S. Havlin, M. Dishon, J. E. Kiefer, and G. H. Weiss, Phys. Rev. Lett. **53**, 407 (1984).

[6] P. Grassberger and I. Procaccia, J. Chem. Phys. **77**, 6281 (1982).

[7] G. H. Weiss, R. Kopelman, and S. Havlin, Phys. Rev. A **39**, 466 (1989).

[8] S. H. Park, H. Peng, S. Parus, H. Taitelbaum, and R. Kopelman, J. Phys. Chem. A **106**, 7586 (2002).

[9] H. Taitelbaum, R. Kopelman, G. H. Weiss, and S. Havlin, Phys. Rev. A **41**, 3116 (1990).

[10] S. Havlin, H. Larralde, R. Kopelman, and G. H. Weiss, Physica A **169**, 337 (1990).

[11] S. Redner and D. Ben-Avraham, J. Phys. A **23**, L1169 (1990).

[12] H. Taitelbaum, Phys. Rev. A **43**, 6592 (1991).

[13] S. H. Park, H. Peng, R. Kopelman, P. Argyrakis, and H. Taitelbaum, Phys. Rev. E **67**, 060103(R) (2003).

[14] H. Taitelbaum, S. Havlin, J. E. Kiefer, B. Trus, and G. H. Weiss, J. Stat. Phys. **65**, 873 (1991).

[15] R. Kopelman and P. Argyrakis, Phys. Rev. E **64**, 017102 (2001).

[16] M. A. Rodriguez, G. Abramson, H. S. Wio, and A. Bru, Phys. Rev. E **48**, 829 (1993).

[17] R. F. Kayser and J. B. Hubbard, Phys. Rev. Lett. **51**, 79 (1983).

[18] A. Giacometti and A. Maritan, Phys. Rev. E **49**, 227 (1994).

[19] S. Mukherjee and H. Nakanishi, Phys. Rev. E **53**, 1470 (1996).

[20] A. D. Sanchez, E. M. Nicola, and H. S. Wio, Phys. Rev. Lett. **78**, 2244 (1997).

[21] Z. Koza and H. Taitelbaum, Phys. Rev. E **57**, 237 (1998).

[22] M. Vlad, F. Spineanu, J. H. Misguich, and R. Balescu, Phys. Rev. E **58**, 7359 (1998).

[23] D. Bar, Phys. Rev. E **64**, 026108 (2001).

[24] R. Descas and K. Mussawisade, Phys. Rev. E **66**, 051103 (2002).

[25] M. V. Smoluchowski, Z. Phys. Chem., **92**, 129 (1917).

[26] A. A. Ovchinnikov and Y. B. Zeldovich, Chem. Phys. **28**, 215 (1978).

[27] D. Toussaint and F. Wilczek, J. Chem. Phys. **78**, 2642 (1983).

[28] R. Kopelman, Science **241**, 1620 (1988).

[29] K. Lindenberg, P. Argyrakis, and R. Kopelman, J. Phys. Chem. **99**, 7542 (1995).

[30] S. Schlipf, H. Katori, L. Perotti, and H. Walther, Opt. Express **3**, 97 (1998).

[31] H. Taitelbaum and Z. Koza, Physica A **285**, 166 (2000).

[32] E. Monson and R. Kopelman, Phys. Rev. Lett. **85**, 666 (2000).

[33] For example, see P. Atkins, *Physical Chemistry*, 7th ed. (Freeman, New York, 1998).

[34] H. S. Carslaw and J. C. Jaeger, *Conduction of Heat in Solids*, 2nd ed. (Oxford University Press, Oxford, 1959).

[35] D. Sinton, D. Erickson, and D. Li, J. Micromech. Microeng. **12**, 898 (2002).